Title

Ultrafast Biomimetic Untethered Soft Actuators with Bone-In-Flesh Constructs Actuated by Magnetic Field

Authors

Yue, Wei
Xu, Renxiao
Sui, Fanping
et al.

Publication Date

2024

DOI

10.1002/adfm.202401159

ADVANCED FUNCTIONAL MATERIALS
www.afm-journal.de

Ultrafast Biomimetic Untethered Soft Actuators with Bone-In-Flesh Constructs Actuated by Magnetic Field

Wei Yue, Renxiao Xu, Fanping Sui, Yuan Gao, and Liwei Lin**

Soft actuators with unique mechanics have gained significant interests for unique capabilities and versatile applications. However, their actuation mechanisms (usually driven by light, heat, or chemical reactions) result in long actuation times. Reported magnetically actuated soft actuators can produce rapid and precise motions, yet their complex manufacturing processes may constrain their range of applications. Here, the "bone-in-flesh" is proposed that constructs combining rigid magnetic structures encapsulated within soft polymers to create untethered magnetic soft actuators. This approach enables these soft, impact-resistant, agile actuators with a significantly simplified fabrication process. As demonstration examples, multiple soft actuators are fabricated and tested, including actuators for auxetic properties, 2D–3D transformations, and multi-stable states. As such, this work offers a promising solution to challenges associated with soft actuators to potentially expand their applications in various domains.

1. Introduction

Studies in soft robots/actuators have drawn widespread interests in recent years.[1–3] Compared with hard-bodied robots/actuators with rigid links and joints, soft and compliant systems can change their shapes to adapt to the external environment and create harmless mechanical interfaces. This feature makes them desirable for applications in various robotic systems, especially those with interactions to biological tissues. Besides, compared with wired, electricity-powered counterparts such as ionic polymer-metal composite (IPMC)[4–6] and dielectric elastomer (DE),[7–9] untethered soft actuators not limited by physical connections, allowing for more freedom of movement and the ability to operate in environments with complex turns and paths. Previously, active polymeric materials including hydrogels, liquid crystal elastomers (LCE), and shape memory polymers (SMP), have been used to make untethered soft actuators with different actuation mechanisms of light, heat, or chemical changes.[10–23] These polymer-based actuators have the desirable soft and compliant mechanics but they generally suffer from slower actuations and more limited precisions when compared with those traditional hard-bodied actuators. Specifically, the key driving mechanisms of these soft actuators are based on slow physical or chemical processes (typically several seconds to hundreds of seconds in the actuation time), including the swelling/shrinking of hydrogels, the heat-induced thermal expansion, the deformation of shape memory polymers, and the external stimulation of liquid crystal elastomers. Furthermore, the actuation precisions in these processes are often compromised by the fluctuations of the external stimuli and changes in the surrounding environment.

While untethered magnetic actuation can result in fast and precise responses, most prior works are based on rigid magnetic structures.[24,25] In recent years, researchers have also reported soft and magnetically controlled actuators across different length scales by embedding ferromagnetic particles with controlled directional magnetization in elastomeric matrices. These actuators have shown desirable actuation speeds and good compliances, but their fabrication processes are rather complex, especially in terms of the magnetization operation: requiring highly-specialized equipment such as a direction-specific 3D printer coupled with accurately timed magnetization processes, or a special lithography process with on-site magnetization.[26–29] In addition, due to the presence of viscous drag within the pre-cured soft material, achieving high-quality magnetization often requires extremely strong external magnetic fields (>1 Tesla) to facilitate a thorough reorientation of magnetic particles.[26–29] In this work, we demonstrate magnetically driven, untethered soft actuators with bone-in-flesh constructs for ultrafast responses with high precisions. Our actuators can be fabricated by simple processes (therefore, no need for specialized facilities for complicated magnetization steps) with low-cost, off-the-shelf magnetic and elastomeric materials.

2. Results and Discussion

2.1. Bioinspired Bone-In-Flesh Constructs

The bone-in-flesh constructs are inspired by examples in living animals such as the human arm, where the rotation of "bones"

W. Yue, R. Xu, F. Sui, Y. Gao, L. Lin
Department of Mechanical Engineering
University of California at Berkeley
Berkeley, CA 94720, USA
E-mail: renxiaoxu@berkeley.edu; lwlin@berkeley.edu

The ORCID identification number(s) for the author(s) of this article can be found under https://doi.org/10.1002/adfm.202401159

DOI: 10.1002/adfm.202401159

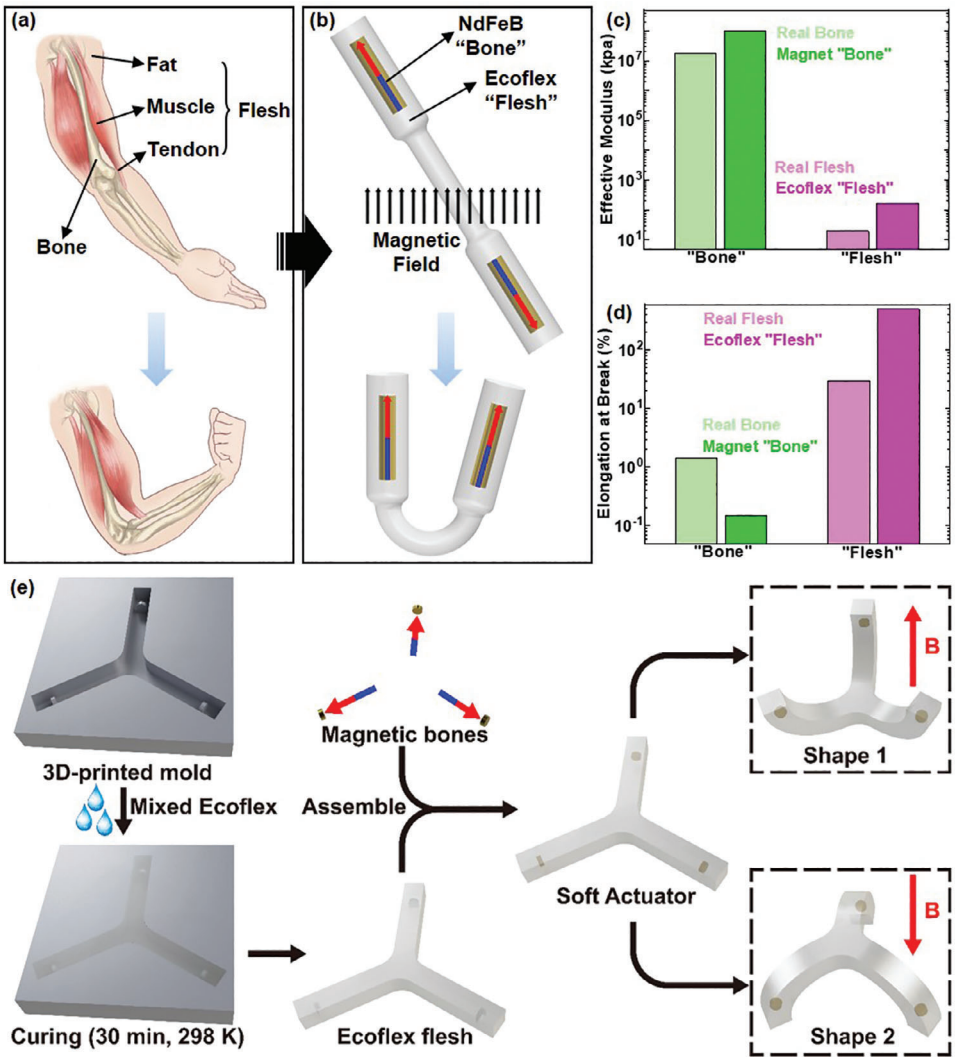

Figure 1. a) The flexing of a human arm, featuring the bones and flesh components. b) Schematics of the working mechanism of a bioinspired bone-in-flesh actuator, with magnets as "bones" and elastomers as "flesh". c) Effective modulus, and d) deformability (evaluated by the amount of elongation at break) of "bone" and "flesh" components in human body and in the proposed actuators. e) Fabrication procedures of bone-in-flesh soft actuators. Mixed Ecoflex is poured into the 3D printed ABS mold, and cured in room temperature for 30 min. The cured Ecoflex flesh is then taken out from the model and inserted with the NdFeB magnetic "bones". After that, the cavities for insertion are enclosed with more Ecoflex. The fabricated soft actuator can deform into different shapes under different external magnetic fields.

facilitates the accurate motions such as flexion and extension, while the "flesh" (including muscles, fat, tendons, and skins) encapsulates and protects the bones from mechanical impacts. The soft flesh also offers a compliant interface as the arm interacts with the surrounding environment (**Figure 1**a). The biomimetic soft actuators use two materials of very different mechanical properties: 1) rigid NdFeB magnets (cylindrical shape, millimeter-scale) as the bones, and 2) highly deformable elastomers (Ecoflex 00–35) as the flesh. An external magnetic field with a flux density, $\boldsymbol{B}$, is utilized to generate an alignment torque $\boldsymbol{\tau} = \boldsymbol{m} \times \boldsymbol{B}$ on the magnet with a magnetic moment of $\boldsymbol{m}$, to actuate the bone-in-flesh construct in a manner similar to the flexion of a human arm, as in Figure 1b. Figure 1c,d shows the mechanical property comparisons between the human arm and the prototype soft actuator, including high moduli (Effective Modulus ≈18 GPa for bones, ≈100 GPa for NdFeB magnets) and brittle mechanics (elongation at break ≈1.43% for bones, 0.15% for NdFeB magnets) core or "bone" materials, and soft and resilient shell or "flesh" materials (Modulus ≈20 kPa and elongation at break ≈30% for human fleshes; Modulus ≈166 kPa, and elongation at break ≈500% for the Ecoflex 00–35 material).[30–34] With carefully engineered combinations of "bone" and "flesh" to be demonstrated in Section 2.2, the actuators could achieve desirable outcome: the "bone" facilitates quick and precise actuation motions, while the soft "flesh" accommodates the large deformations and alleviates mechanical impacts.

The bone-in-flesh construct uses a simple fabrication process as shown in Figure 1e without any special tool such as equipment used for patterning with directional magnetization. In the prototype fabrication process, a standard FDM 3D printer

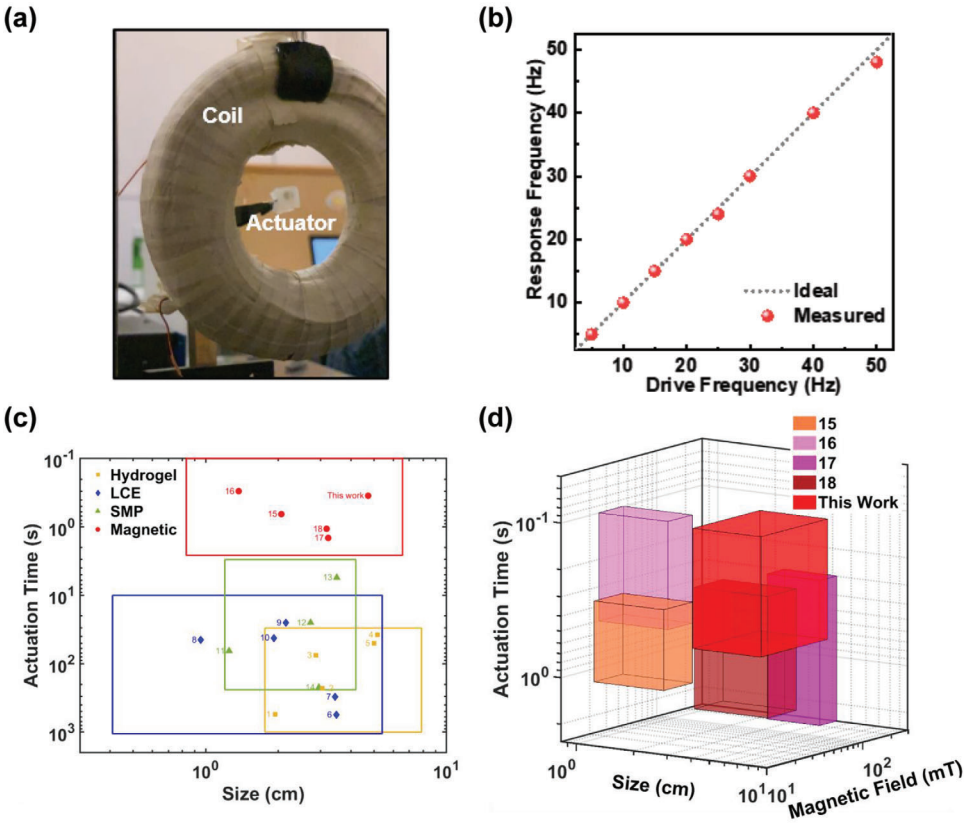

Figure 2. a) Experimental setup for testing an actuator's response under an alternating magnetic field. b) Response versus driving frequency of an actuator, as read from video images at 240 frames per second. The magnetic field flux density is ≈20 mT. c) Comparison in actuation time between magnetically powered soft actuators and actuators of similar length scale using other working mechanisms. Each rectangle represents a category of soft actuators, each point represents a work (mean value). The annotated numbers correspond to the numbers in Table S1 (Supporting Information). d) Comparison in actuation time among different magnetically powered soft actuators.

(*Stratasys Dimension*) and common materials (ABS filaments, Ecoflex 00–35, and neodymium magnets of various sizes and grades) are used. First, an ABS part is printed by the 3D printer to serve as the mold with protrusions as the slots for magnet insertions in a later step. Ecoflex is poured into the mold in the liquid state and cured at room temperature to form the "flesh" part of the actuator. Finally, several cylindrical NdFeB magnets with chosen polarities are inserted into the predesigned slots to act as "bones" and sealed by Ecoflex to finish the fabrication. The external magnetic field can deform the soft actuators to result in different shapes in an ultrafast fashion for the actuation.

To evaluate the agility of the bone-in-flesh actuators, a prototype sample is placed in an alternating magnetic field by using the magnetic coil structure (**Figure 2a**). The magnet as the "bone" will align its polarity with the sinusoidal alternating magnetic field with an amplitude ≈20 mT, leading the entire structure to deform periodically as recorded by a video camera at 240 frames per second. Figure 2b shows the response frequency versus the driving frequency results up to 50 Hz, which is considered fast enough for most applications. It is observed that the actuator can catch up with the 50 Hz alternating magnetic field, indicating the typical response time of less than 0.02 s. The full actuation time for a prototype actuator to change from its initial shape to the fully deformed configuration is between 0.1 and 0.6 s depending on the specific structure under a magnetic field ranging from 20 to 100 mT. Figure 2c presents a comparison of actuation times for centimeter-scale untethered soft actuators made of hydrogels,[10–14] liquid crystal elastomers (LCEs),[15–18] shape memory polymers (SMPs),[20–23] and previously-reported magnetic soft actuators,[26–29] where the same type of actuators are denoted by the same color. It is evident that magnetic soft actuators achieve a faster actuation compared with other types of untethered soft actuators. Figure 2d and Table S1 (Supporting Information) show a further comparison in actuation time, size, and required magnetic flux density for actuation, within the category of magnetic soft actuators. While our bone-in-flesh actuators are fabricated in a simple process without using special tools, they yield roughly the same, if not shorter, actuation time to other soft magnetic actuators using more complex procedures, when the dimensions and magnetic fields are comparable.

One major advantage of soft actuators over their more rigid counterparts is the ability to accommodate harsh mechanical impacts through recoverable material deformation. In robotics applications, typical mechanical impacts include sudden drops from a considerable height, unexpected collisions by heavy objects, and applied concentrated or distributed loads. We

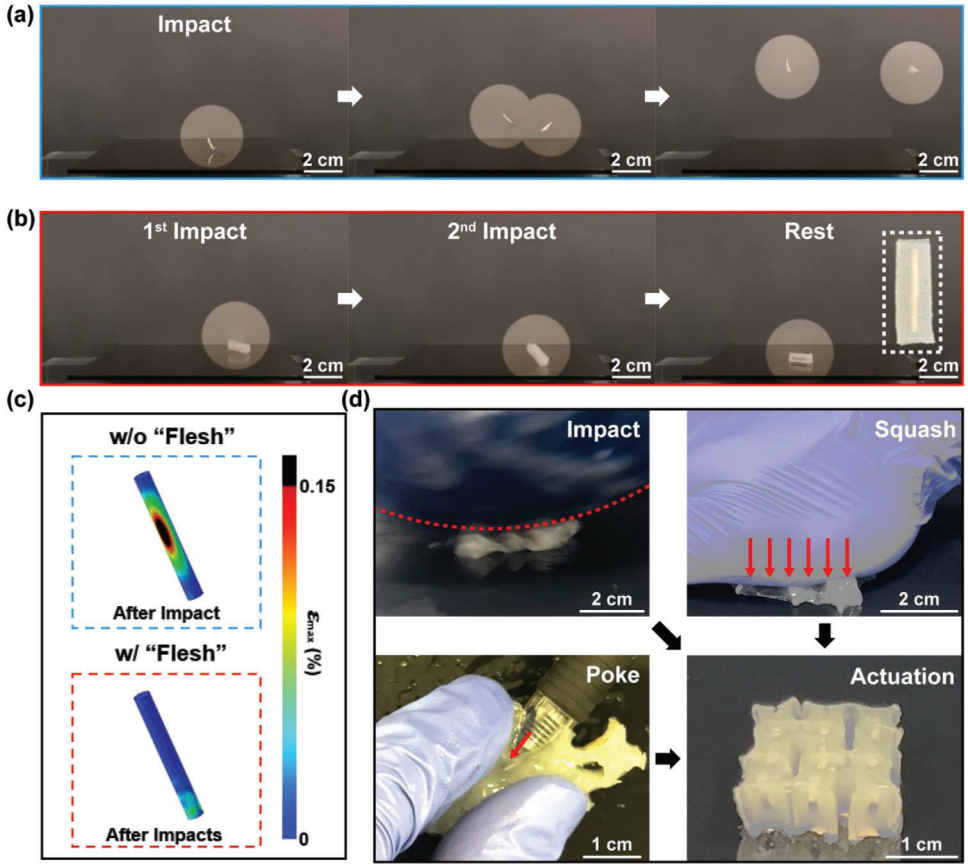

Figure 3. a,b) Recorded sequential images during a free-fall drop test, for a column-shaped magnet (a) without and (b) with the encapsulating elastomeric "flesh". The inset in (b) shows the intact structure after the test. c) Maximum principal strain distribution on the magnet (without or with "flesh") after impact(s) computed by FEA. d) Images of different mechanical impact tests on a representative actuator including heavy object impacts (top left), squashing (top right), and poking by sharp objects (bottom left). The actuator remains fully functional after these tests (bottom right).

conducted the following experiments to mimic these mechanical impacts and test the reliability of our soft actuators. **Figure** 3a,b shows distinct responses of two samples when dropped onto a rigid floor made of quartz from a height of 1.3 meters. While a bare cylinder-shaped magnetic "bone" cracks into two pieces upon hitting the floor (Figure 3a; Supplementary Movie S1, Supporting Information), a magnetic "bone" of the same size and shape could easily survive multiple impacts when encapsulated by the soft and deformable Ecoflex "flesh" (Figure 3b; Supplementary Movie S1, Supporting Information). Finite element analysis (FEA) also confirms that the max principal strain in the magnetic "bone" exceeds fracture limit considerably (≈0.15% for NdFeB) when the bare sample hits the floor, while the principal strain remains far below the fracture limit throughout the drop event of the bone-in-flesh sample (Figure 3c). This test proves that the "flesh" material shields the brittle "bone" from damage and provides great resilience to mechanical impacts for a bone-in-flesh construct. We then conducted a series of extreme reliability tests on a representative bone-in-flesh actuator (Figure 3d). In one test, the actuator was subject to the full impact of a Bowling ball (5352 gram, over 1000 times heavier than the actuator) released at a height of 30 cm (Supplementary Movie S2, Supporting Information). In other tests, the actuator was squashed and flattened by a palm, or significantly poked by a ballpoint pen (Supplementary Movies S3 and S4, Supporting Information). Despite severe changes in shape during the three tests, the deformation was fully recoverable. Once the impacts and loads were removed, the actuator returned to its initial form, and retained its full functionality in response to an external magnetic field.

In the following sections, four classes of actuators all with bone-in-flesh constructs have been demonstrated for various potential applications. In these actuators, the rotation of "bones" in the magnetic field initiates and powers the actuation, while the compliant "flesh" with carefully engineered structures changes the shape accordingly to complete the large overall deformations. The first three demonstration examples reflect recent advances in modern mechanics and mechanical metamaterials, including the auxeticity,[35–38] 2D-to-3D transformation,[24,39–45] and bistable/multi-stable structures,[45–47] while the last example (a soft gripper) targets practical application scenarios.

2.2. Actuators for Auxetic Contraction and Expansion

Auxeticity, or the property of having a negative Poisson's ratio, is a hot research topic in mechanical metamaterials.[35–38] Here, devices for auxetic actuation in an untethered manner with ultrafast actuations are demonstrated. **Figure** 4a,b shows two

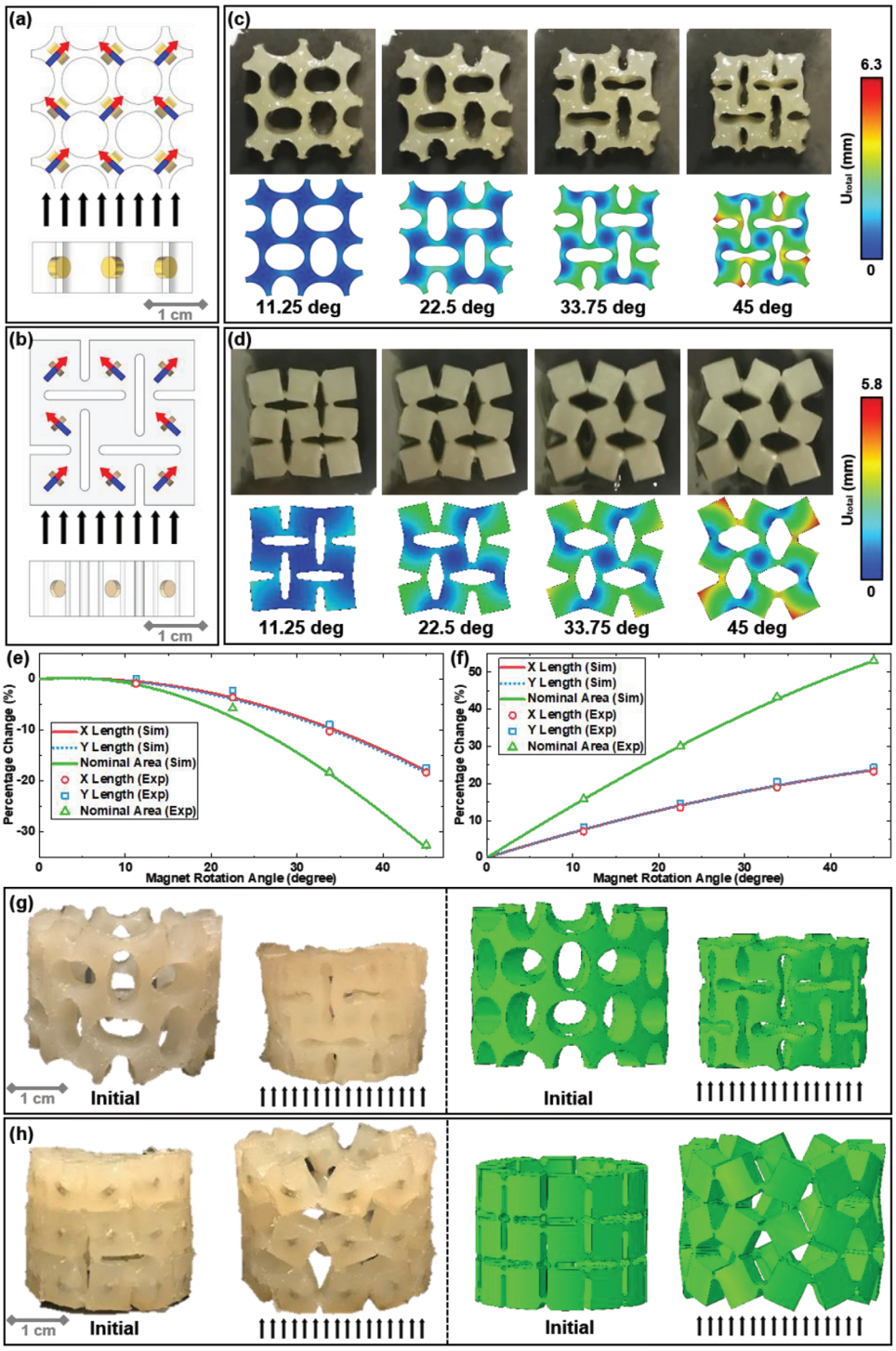

Figure 4. a) Schematics of soft actuators for 2D auxetic contraction, in top and side views. The red/blue arrows denote the polarity of magnets, and the scale bar is 1 cm. b) Schematics of soft actuators for 2D auxetic expansion, in top and side views. The red/blue arrows denote the polarity of magnets, and the scale bar is 1 cm. c) Recorded (top row) and computed (bottom row) deformation of the actuator for contraction, during four representative stages. d) Recorded (top row) and computed (bottom row) deformation of the actuator for expansion, during four representative stages. e) Percentage decrease in lengths and nominal area versus the rotation angle of magnets during the contraction actuation, as predicted by FEA (lines) and measured in experiments (dots). f) Percentage increase in lengths and nominal area versus the rotation angle of magnets during the expansion actuation, as predicted by FEA (lines) and measured in experiments (dots). g) Recorded (left) and computed (right) deformation of the actuator for 3D auxetic contraction. h) Recorded (left) and computed (right) deformation of the actuator for 3D auxetic expansion. The magnetic field strength is ≈56 mT for (c, d) and ≈100 mT for (g,h). For panels (c) and (d), colors in FEA results denote total displacement.

actuators with "flesh" (semitransparent) and "bones" (in golden metallic color) for 2D auxetic actuations. The top and side views show the highlighted blue and red arrows pointing from the south to the north pole inside each magnetic "bone". Both actuators have a width and length of 3 cm, and a thickness of ≈1 cm. In the elastomeric "flesh", the device for the contraction motion (Figure 4a) has four large circular holes near the center and several peripheral semi- and quarter- circular features. The device for the expansion motion (Figure 4b) has alternating horizontal and vertical slots through its thickness. When an external magnetic field (≈56 mT, denoted by black arrows) is applied, the magnetic "bones" with polarities offset from the applied field will rotate by 45° under the alignment torque, causing the deformation of the structured "flesh". With a rational combination of adequately strong magnetic field (no less than ≈56 mT) and compliant enough "flesh" material (modulus <166 kPa) identified through FEA, the actuators could achieve a "sufficient actuation", featured by the magnetic "bones" rotating by 45° or more to fully align their polarities with the external field during the dynamic process. (detailed in Supplementary Note S1, S2, and Figure S1, Supporting Information). In the actuator for contraction, the four circular holes are gradually squeezed into alternately arranged ovals, and later dumbbell shapes, letting the entire structure reduce its nominal area within 0.2 s (Figure 4c). Over a "sufficient actuation" process, the lengths in both planar directions (X and Y) shrink simultaneously by 18.5%, hence yielding a negative Poisson's ratio of ≈−1 (Figure 4e). The total reduction in the nominal area is ≈33%. Upon the removal of the external magnetic field, the structure rapidly releases its elastic potential energy, and returns to its initial state within 0.2 s. The deformation and recovery processes are shown by Supplementary Movie S5 (Supporting Information). In another device driven by the 45° rotation of magnetic "bones", the slender slots in the elastomeric "flesh" are stretched into alternately arranged rhombic voids within 0.3 s, such that the nominal area of the actuator is enlarged by ≈53% (Figure 4d,f). The lengths in both X and Y are increased by ≈24%, again indicating the 2D auxetic nature of this actuation process. The structure can also recover to its initial state after the removal of the external field within 0.4 s (Supplementary Movie S6, Supporting Information). For both actuators, the deformations predicted by FEA match those observed in experiments, not only in visual features (Figure 4c,d), but also in the quantitative results (Figure 4e,f).

Periodic repetition of the structures in the aforementioned two actuators can be done on a plane for large 2D actuators. This repetition can also be performed on an open cylindrical surface to achieve 3D auxetic actuation. Figure S2 (Supporting Information) illustrates such actuators, each involving 36 magnetic "bones". For the contractable structure, the circular holes are slightly modified into alternating elliptical shapes for smoother transformation. Figure 4g, demonstrate the shapes of the actuators in their initial configurations, and in the deformed shapes after ≈0.4 s in constant magnetic field (≈100 mT), including the experimental images (left column) and FEA models (right column). We observe the apparent simultaneous decrease (or likewise increase) in length in the expected axial and hoop directions (i.e., height and circumference), as well as in the third, radial direction. Such results show that these two devices indeed actuate in a 3D auxetic way. Notably, the amount of rotation for magnetic "bones" is less than 45° in these 3D actuators, as the features near the inner surface will eventually come into physical contact among themselves and prevent further deformation. Such effect is both considered in FEA models and recorded in experiments.

2.3. Actuators for 2D-to-3D Shape Transformation

The assembly of 2D planar patterns into complex 3D shapes is another trending research theme. Two most popular approaches for the 2D-to-3D transition across multiple length scales are: 1) utilizing the compressive buckling of thin films partially adhered to elastomeric substrates upon releasing the substrate pre-stretch energy,[39–41] and 2) applying the folding of thin films along predesigned traces (also known as "Origami") upon applying mechanical force and other physical/chemical stimuli.[24,42–45] Here we present three bone-in-flesh actuators for magnetically powered 2D-to-3D shape transformation, each representative of a unique strategy.

The first actuator achieves the transformation through the bending of selective "flesh" parts due to differences in bending stiffness. As illustrated in **Figure 5a**, the structured "flesh" is composed of nine blocks, connected by thinner and narrower segments among them. Four magnetic "bones" are strategically embedded in the corner blocks with specifically chosen polarities. The polarities of two bones (group 1) are set to be exactly opposite to the other two (group 2), ensuring bones in the two groups to rotate in opposite directions. Upon an applied magnetic field (≈100 mT) and due to the large difference in the bending stiffness (≈10 times) between segments and blocks, a considerable overall out-of-plane displacement is achieved, forming a 3D shape in ≈0.17 s (Supplementary Movie S7, Supporting Information). Depending on the direction of the magnetic field, the actuator can transform between two different 3D gestures: 1) a state resembling a "butterfly" featuring high left/right and low front/back blocks under an upward magnetic field, and 2) a "saddle" state characterized by low sides and high front and back blocks under a downward magnetic field (Figure 5b). The recorded deformation agrees with FEA calculations excellently to subtle details. From FEA results, it is found that the actuator reaches up to ≈2.6 times of its height during the 2D-to-3D transformation, with the in-plane diagonal length reduced by 28.5% (Figure 5c). In this example, the stiffness of the flesh is significant enough to partially overcome the alignment torque exerted by the magnetic field, setting it apart from other samples. Its stable configuration does not involve aligning with the external magnetic field in a nearly parallel orientation. A detailed theoretical model to analyze the deformation of this structure is developed (See Supplementary Note S3, Supporting Information), enabling a more accurate prediction of the deformation under a given magnetic field magnitude.

With more pronounced differences in thickness (hence bending stiffness) within the structure, an event similar to paper-folding, or "Origami", can occur.[39] Figure 5d illustrates a device actuated by the concept of Origami, where the elastomeric "flesh" is structured into a thin (≈0.25 mm) membrane and thick (additional ≈1.4 mm) triangular or rectangular mesas above it. When a magnetic field is applied, the rectangular mesas with embedded "bones" quickly (within ≈0.5 s) rotate to render almost perpendicular sidewalls, while the thin regions of "flesh" serve as

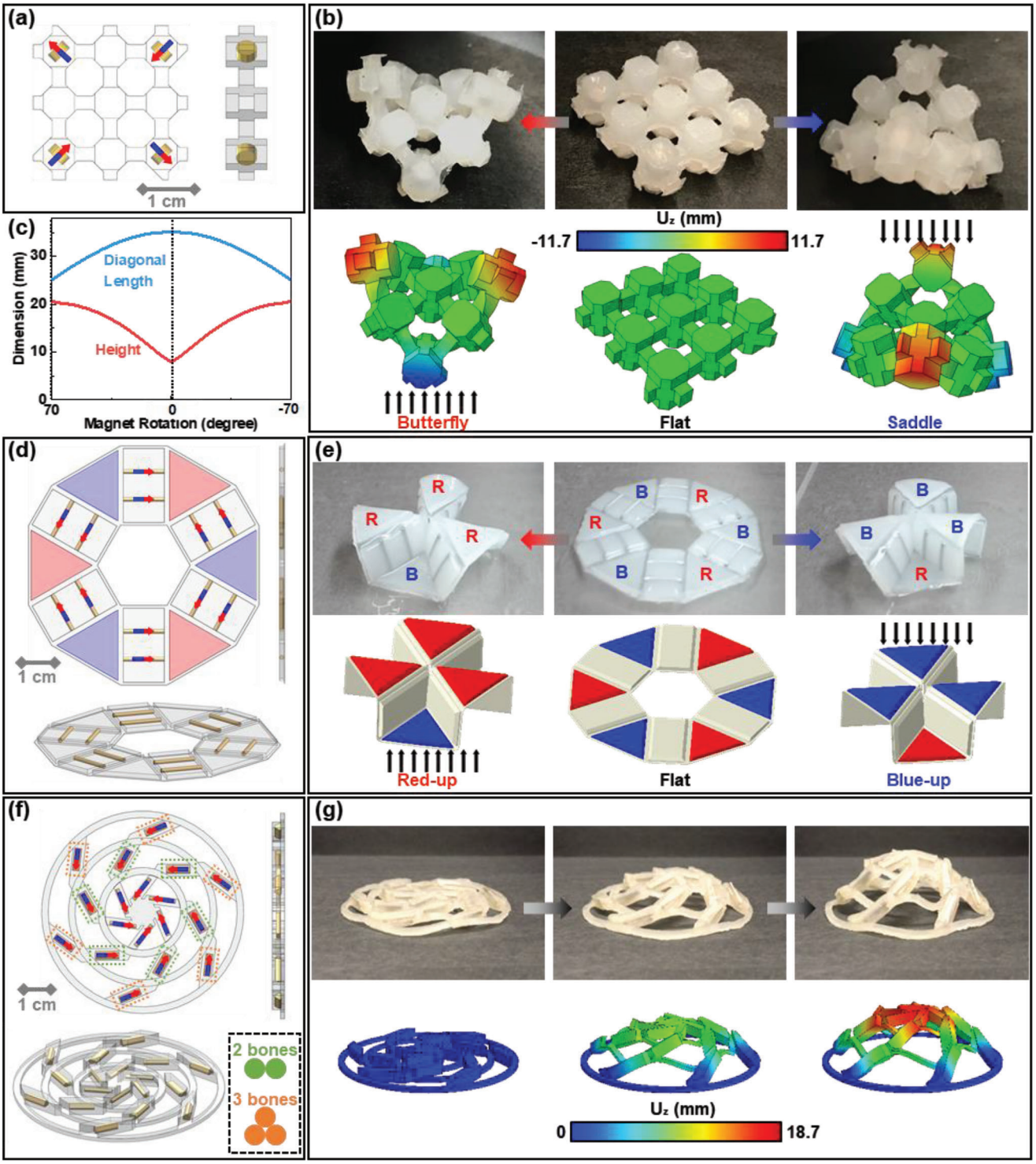

Figure 5. a) Schematics of a soft actuator for bending-based 2D-to-3D transformation, in top and side views. b) Recorded (top column) and computed (bottom column) transitions among the "butterfly" state, the undeformed flat state, and the "saddle" state. c) Changes in height and length versus magnet rotation angle during the actuation process. d) Schematics of a soft actuator for origami-type 2D-to-3D transformation, in top, side and tilted 3D views. e) Recorded (top column) and computed (bottom column) transitions among the "Red-Up" state, the undeformed flat state, and the "Blue-Up" state. In photos, the letters "R" and "B" denote red and blue faces, respectively. f) Schematics of a soft actuator with magnet bundles for 2D-to-3D transformation, in top, side and tilted 3D views. The inset shows a cross-sectional profile of a two-bone and a three-bone bundle. g) Recorded (top column) and computed (bottom column) deformations during the actuation process. The magetic field strength is ≈100 mT for (b), (e), and (g). For panels (b) and (g), colors in FEA denote out-of-plane displacement.

the creases for reversible foldings (Figure 5e). Under an upward magnetic field (1st column in Figure 5e), one set of triangular mesas lifts up (marked as red in Figure 5d,e) to form the ceiling in the generated 3D structure, while the other set (marked as blue) stays low to form the ground. In a second situation by reversing the applied magnetic field (3rd column in Figure 5e), the magnetic "bones" will rotate in opposite directions with the set marked as blue moving up instead to form a reversed structural configuration. As shown in Supplementary Movie S8 (Supporting Information), the structure has the ability to swiftly recover its shape (within ≈0.4 s) upon removal of the external magnetic field (≈100 mT) in both situations. Through incorporating mesas with diverse shapes and sizes in the "flesh", and placing various magnetic "bones" at different sites, these soft actuators could potentially assemble into numerous intriguing 3D Origamis, with the desirable rapid actuations, easily reversed shapes, and recoverable nature.

The third actuator for 2D-to-3D transformation involves the idea of bundling two or three parallel magnetic "bones" (Figure 5f), with some geometric similarities to the parallel radius and ulna in human's forearm. Concentrating multiple magnetic "bones" together increases the magnetic moment, thereby enhancing the alignment torque. In the actuator, these "bone" bundles reside in the thicker and wider segments of "flesh", to facilitate bending in these stiffer regions by providing doubled or tripled alignment torque. In this actuator, six single "bones", six two-bone bundles, and six three-bone bundles constitute the entire skeleton. Figure 5g shows the transformation process of this actuator under a maximum magnetic field of ≈100 mT, from an almost flat shape into a 3D complex object resembling the well-known Bird's Nest Stadium in Beijing. In this demo, we intentionally moved the magnet source inward and outward slowly (in ≈1 s), making the deformation and recovery of the actuator a quasi-static process, as captured in Supplementary Movie S9 (Supporting Information). Potentially, a vast variety of 3D structures with more convoluted geometries and curvilinear details could be quickly assembled by this type of bone-in-flesh actuators, through the inclusion of assorted bundling of "bones" and diverse shapes of "flesh" during the design process.

2.4. Actuators with Bistable or Multi-stable States

A third type of actuators built upon the bistable and multi-stable structures.[45–47] **Figure 6a** illustrates the structure of a bistable pop-up switch, with the four magnetic "bones" embedded in the thick, annular portions of the "flesh". Initially, the switch is without deformation at the "up" position (Figure 6b(i)). After the switch is pressed elastically downward by an external force to the preset maximum displacement (Figure 6b,(ii)), it would not return to the "up" position even after the applied load is retracted. Instead, the switch remains locked at a "down" position (Figure 6b(iii)), until the device is actuated by an external magnetic field (≈100 mT) for resetting back to the "up" position (Figure 6b(iv); Supplementary Movie S10, Supporting Information). Figure 6e shows the elastic strain energy E and the applied force F corresponding to different stages in the loading and unloading process, as calculated from FEA, where the displacement is normalized. The "up" position is the first stable state (State 1) with elastic strain energy $E_1 = 0$, while the "down" position is a second stable state (State 2) with elastic strain energy E_2 at a local minimum. With the applied force F gradually retracted to zero, the system only recovers to the "down" position (State 2) instead of all the way to the "up" position (State 1), because of the energy barrier near State 2. An amount of elastic strain energy equal to E_2 is therefore trapped in the system. With the applied magnetic field driving the "bones" to provide this system with the additional energy, the system can overcome the energy barrier and reset to its initial configuration.

Actuators for the transitions among multiple stable states are also realized by using a conical membrane with predesigned thickness variations as "flesh", and 24 small column-shaped magnets as "bones" (Figure 6c). The thin regions in the membrane can fold inward or remain straight to result in two different shapes. In total, this actuator has four stable configurations, namely State 1, 2, 3, and 4, with corresponding elastic strain energy $0 = E_1 < E_2 < E_3 < E_4$. At each stable state, the elastic strain energy is at the global or a local minimum, and the force transitions from zero to positive (Figure 6d,f). Applying a downward force by a finger at the top center of the structure shifts the system to the immediate next configuration with higher strain energy (forward purple arrows), while the magnetic actuation (magnetic flux density ≈100 mT) can reset the system to the previous neighboring state (backward gray arrows). Here, small magnets with low magnetic grade are deliberately chosen to avoid the cross transformation between two nonadjacent states. Multi-stable systems like this represent a step toward bone-in-flesh actuators imitating the biological structures with multiple joints in series (e.g., the arm and hand of human), where each joint can rest in either flexed or extended positions.

2.5. A Soft Gripper

As a last example, a six-fingered, soft gripper that tightens or opens within 0.1 s is demonstrated, when subject to a forward or a reversed external magnetic field (**Figure 7a,b**). The alignment torque on the magnetic "bones" provides sufficient force for the reliable gripping of objects. The magnets are embedded near the base (the mutual interference between magnetic "bones" is negligible as explained in Supplementary Note S4, Supporting Information) and the six fingers are made of soft "flesh" completely in order to adapt to various shapes of objects without applying excessive pressure. Experiments have been conducted to test the gripper's capability of dexterous grasping and manipulation of small objects. In the first experiment (Figure 7c), the gripper is positioned above the 3D-printed letter "R" of the word "TRANSDUCERS", made of ABS and weighs ≈0.3 grams. In a downward magnetic field (≈100 mT), the gripper picks the letter up, and holds it during the transportation process to another site. Afterward, the gripper opens its fingers under an upward magnetic field (≈100 mT) to release the object. In similar experiments, we have successfully used the gripper to pick up and transfer heavier objects, such as a peanut (0.8 gram, Figure 7d), a screw bolt (4.5 gram, Figure 7e), and a set of nut, washer and bolt (9.0 gram, Figure 7f). We envision that more challenging tasks such as the manipulations of heavy, brittle, slippery or weird-shaped objects could be completed by other soft grippers with bone-in-flesh

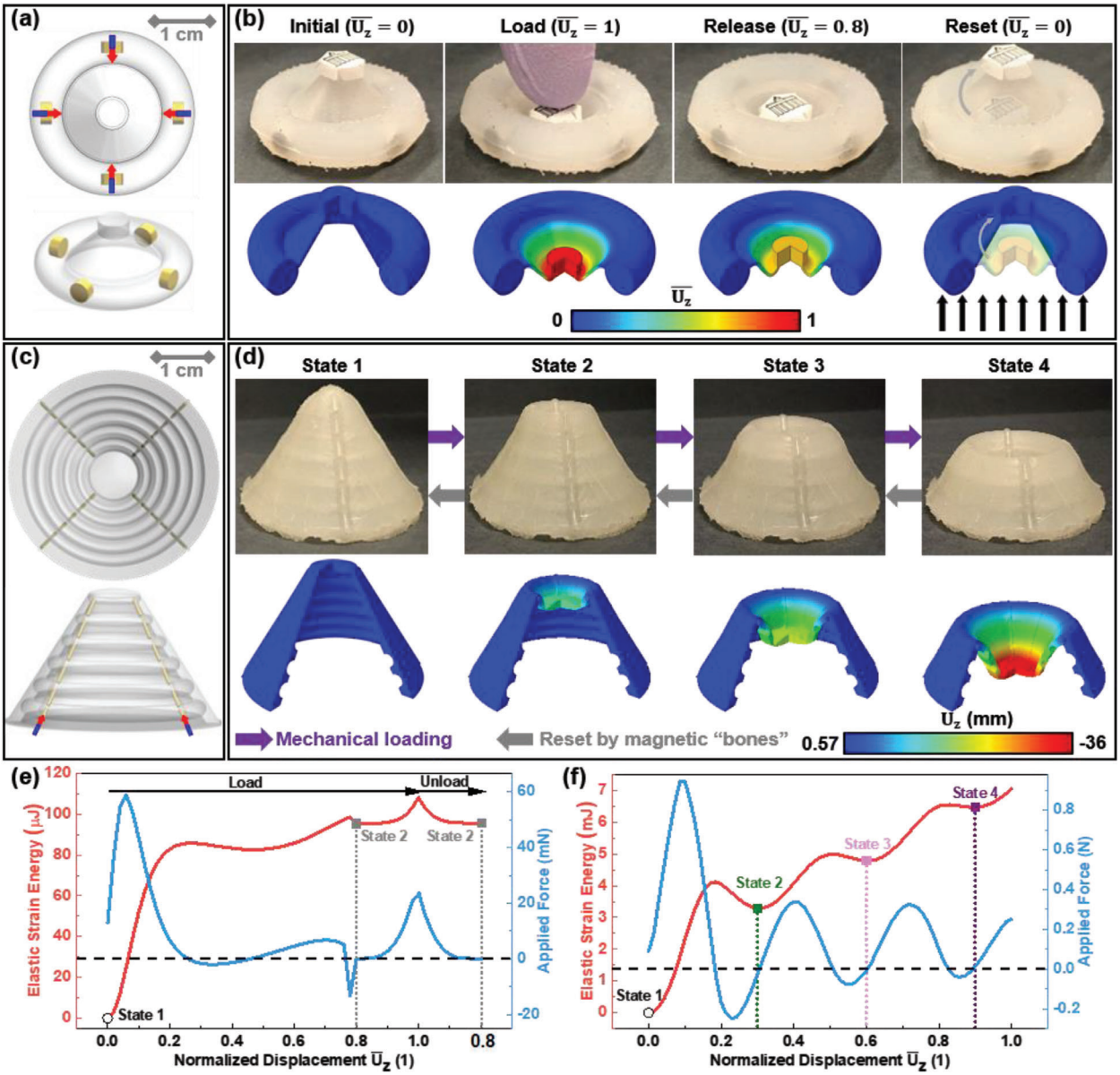

Figure 6. a) Schematics of a bistable, pop-up switch, in top and 3D tilted views. b) Recorded (top row) and computed (bottom row) images for the process of mechanical loading/unloading (first three columns) and magnetically powered reset (last column). Colors in FEA denote normalized out-of-plane displacement. c) Schematics of a multi-stable tower, in bottom and 3D tilted views. The red/blue arrows denote the representative polarity of magnets. d) Recorded (top row) and computed (bottom row) images showing the four stable states of the system in (c). Colors in FEA denote out-of-plane displacement. e,f) Elastic strain energy and applied force versus normalized displacement in the z-direction for (e) the bistable, pop-up switch, and (f) the multi-stable tower. The magetic field strength is ≈100 mT for (b) and (d).

constructs through rational improvements, such as including more magnetic "bones" to form multiple joints and optimizing the structures of elastomeric "flesh", etc.

3. Conclusion

This work reports a bioinspired bone-in-flesh construct for building magnetically powered and untethered soft actuators. This integration of commercial off-the-shelf soft and hard materials into engineered structures not only renders fast and precise actuations with desirable compliant and impact-resistant mechanics, but also remarkably simplifies their fabrication procedures. The demonstrated devices have achieved several distinct functions, including four different auxetic expansions or contractions, three types of planar to out-of-plane transformations, actuation among bistable and multi-stable states, and the manipulation of small objects by a gripper structure. In the future, the bioinspired hard-soft integrated designs can be expanded using the simple fabrication procedures to accomplish more complex tasks, with the ultimate goal of building

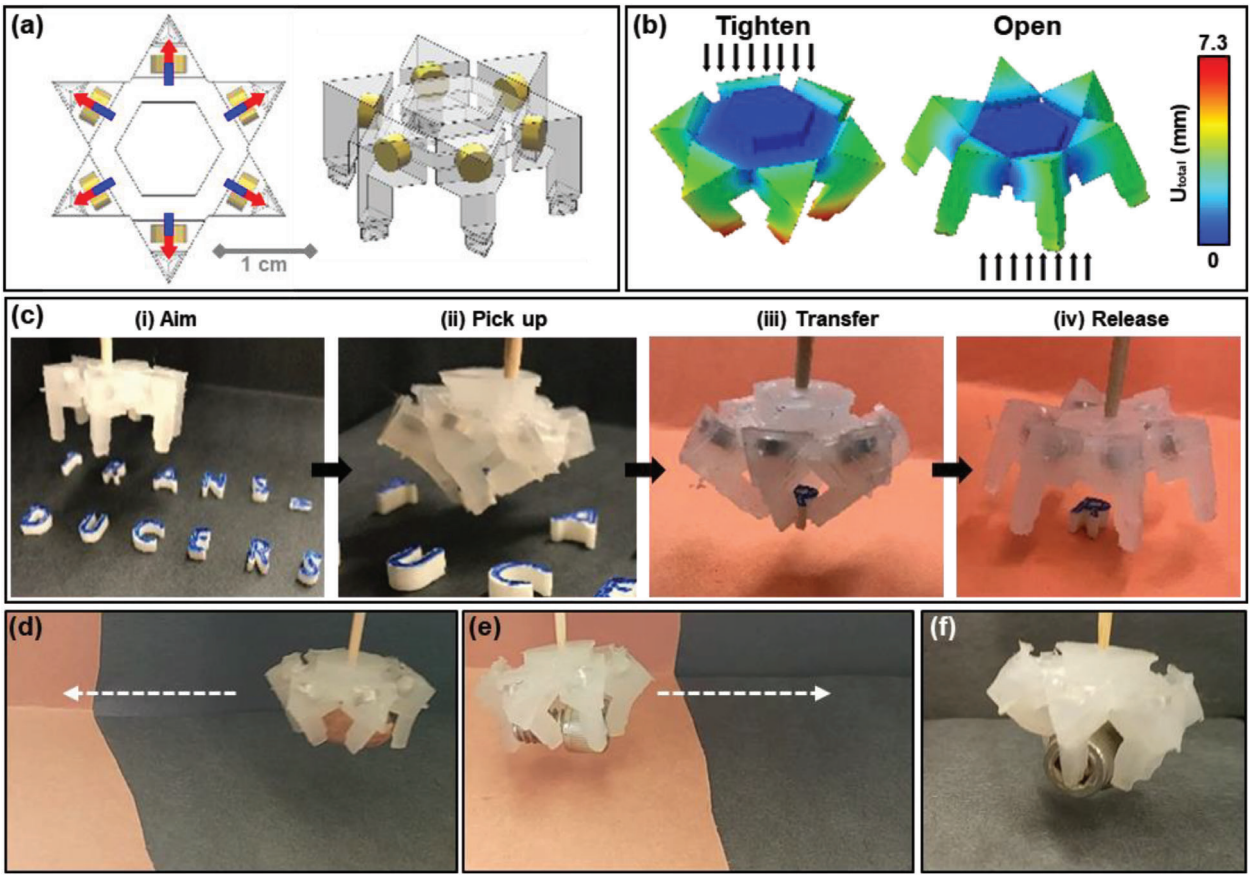

Figure 7. a) Schematics of a six-fingered bone-in-flesh gripper, in top and 3D tilted views. b) FEA-predicted deformation in the tightening and the opening modes. Colors denote total displacement. c) Optical images demonstrating the grasping, transferring and release of a small object. d–f) Optical images of the gripper manipulating (d) a peanut, (e) a screw bolt and (f) a set of nut, washer and bolt. The magetic field strength is ≈100 mT for (c–f).

multifunctional bone-in-flesh soft robots to emulate their biological counterparts.

4. Experimental Section

Magnets for Actuators: Cylindrical NdFeB magnets with different sizes and grades are used for specific actuation requirements. The magnetic moment, $\boldsymbol{m}$, describing the magnetic strength of a certain magnet, is proportional to the magnet's volume, V, and remanence, $\boldsymbol{B_r}$ as $\boldsymbol{m} = (1/\mu_0)\,\boldsymbol{B_r V}$, where μ_0 is the permeability of vacuum. Commercial magnets of higher grades (e.g., N42) have higher remanence than those of lower grades (e.g., N35). Therefore, magnets with higher grade and larger volumes (e.g., N52 with the diameter of 1 mm and length of 1 mm, N48 with the diameter of 4 mm and length of 2 mm, N48 with the diameter of 3 mm and length of 2 mm, N42 with the diameter of 1.59 mm and length of 12.7 mm) are used for most devices for fast and large deformations. Lower grade and small magnets (N35 with the diameter of 1 mm and length of 5 mm) are used for the multi-stable tower demonstration. In addition, slender, cylindrical-shaped magnets are used in thin membranes for large out-of-plane displacements, while stubby, disk-shaped magnets are inserted in bulkier portions of the "flesh" for in-plane-dominated deformations.

Ecoflex Flesh: All soft actuators use Ecoflex 00–35 as the flesh material. First, the required mass of Ecoflex for the soft actuator is estimated and divided into corresponding masses of Part A and Part B. They are premixed and blended in a container. Ecoflex 00–35 has a pot life of 2.5 min, so it needs to be poured into the container and degassed before solidifying. Although the cure time for Ecoflex 00–35 is only 5 min, it was cured for 30 min at room temperature to ensure the complete solidification. The molds designed for each soft actuator are demonstrated in Figure S3 (Supporting Information).

Applying External Magnetic Field: A cubic N52 NdFeB magnet with an edge length of 25.4 mm is utilized to apply the external magnetic field. Depending on the type of soft actuator, three different experimental setups are employed as illustrated in Figure S4 (Supporting Information). Both 2D auxetic contraction and 2D auxetic expansion actuators are actuated by using a fringing magnetic field as shown in Figure S4a (Supporting Information), with a magnetic field parallel to the platform. Most other soft actuators are actuated by using a perpendicular field (normal field) as shown in Figure S4b (Supporting Information), with a magnetic field perpendicular to the platform. The 3D auxetic contraction and 3D auxetic expansion actuators are actuated using a more uniform magnetic field perpendicular to the platform between the two external magnets as shown in Figure S4c (Supporting Information). In all tests, cubic N52 permanent magnets (25.4 mm by 25.4 mm by 25.4 mm) are used to achieve good actuation performances within a distance of 2–3 cm away and the corresponding magnetic field strengths are simulated in Figure S5 (Supporting Information).

Supporting Information

Supporting Information is available from the Wiley Online Library or from the author.

Acknowledgements

W.Y. and R.X. contributed equally to this work. This project was supported by the Berkeley Sensor and Actuator Center. The authors thank Peisheng He, Zhe Ma, Liangjie Ren, Guangchen Lan, Gaurav Jalan, and Pinghsun Lee for discussions and assistance.

Conflict of Interest

The authors declare no conflict of interest.

Data Availability Statement

The data that support the findings of this study are available from the corresponding author upon reasonable request.

Keywords

bone-in-flesh, fast actuation, magnetically powered, soft actuator, untethered

Received: January 19, 2024
Revised: April 1, 2024
Published online:

[1] M. Li, A. Pal, A. Aghakhani, A. Pena-Francesch, M. Sitti, *Nat. Rev. Mater.* **2022**, *7*, 235.
[2] C. D. Santina, C. Duriez, D. Rus, *IEEE Control Syst.* **2023**, *43*, 30.
[3] Y. Zhai, A. De Boer, J. Yan, B. Shih, M. Faber, J. Speros, R. Gupta, M. T. Tolley, *Sci. Robot* **2023**, *8*, eadg3792.
[4] Q. He, Z. Liu, G. Yin, Y. Yue, M. Yu, H. Li, K. Ji, X. Xu, Z. Dai, M. Chen, *Smart Mater. Struct.* **2020**, *29*, 045013.
[5] S. Ma, Y. Zhang, Y. Liang, L. Ren, W. Tian, L. Ren, *Adv. Funct. Mater.* **2020**, *30*, 1908508.
[6] L. Yang, D. Zhang, H. Wang, X. Zhang, *Adv. Eng. Mater.* **2020**, *22*, 2000537.
[7] M. W. N. Tan, H. Bark, G. Thangavel, X. Gong, P. S. Lee, *Nat. Commun.* **2022**, *13*, 6769.
[8] J. Xu, Y. Dong, Z. Jiang, L. Tang, X. Chen, Z. Yao, K. Cao, *Composites, Part A* **2021**, *149*, 106519.
[9] J. Pu, Y. Meng, Z. Xie, Z. Peng, J. Wu, Y. Shi, R. Plamthottam, W. Yang, Q. Pei, *Sci. Adv.* **2022**, *8*, eabm6200.
[10] S. Wei, W. Lu, X. Le, C. Ma, H. Lin, B. Wu, J. Zhang, P. Theato, T. Chen, *Angew. Chem., Int. Ed.* **2019**, *58*, 16243.
[11] Z. Shao, S. Wu, Q. Zhang, H. Xie, T. Xiang, S. Zhou, *Polym. Chem.* **2021**, *12*, 670.
[12] W. Xu, P. Dong, S. Lin, Z. Kuang, Z. Zhang, S. Wang, F. Ye, L. Cheng, H. Wu, A. Liu, *Sens. Actuators, B* **2022**, *359*, 131547.
[13] P. Chen, Q. Ruan, R. Nasseri, H. Zhang, X. Xi, H. Xia, G. Xu, Q. Xie, C. Yi, Z. Sun, H. Shahsavan, W. Zhang, *Adv. Sci.* **2022**, *9*, 2204730.
[14] P. Xue, H. Bisoyi, Y. Chen, H. Zeng, J. Yang, X. Yang, P. Lv, X. Zhang, A. Priimagi, L. Wang, X. Xu, Q. Li, *Angew. Chem., Int. Ed.* **2020**, *60*, 3390.
[15] A. Kotikian, J. M. Morales, A. Lu, J. Mueller, Z. S. Davidson, J. W. Boley, J. A. Lewis, *Adv. Mater.* **2021**, *33*, 2101814.
[16] J. Sun, W. Liao, Z. Yang, *Adv. Mater.* **2023**, *35*, 2302706.
[17] J.-H. Lee, J. Bae, J. H. Hwang, M.-Y. Choi, Y. S. Kim, S. Park, J.-H. Na, D.-G. Kim, S.-k. Ahn, *Adv. Funct. Mater.* **2022**, *32*, 2110360.
[18] Y. Wang, R. Yin, L. Jin, M. Liu, Y. Gao, J. Raney, S. Yang, *Adv. Funct. Mater.* **2023**, *33*, 2210614.
[19] K. Kim, Y. Guo, J. Bae, S. Choi, H. Y. Song, S. Park, K. Hyun, S.-K. Ahn, *Small* **2021**, *17*, 2100910.
[20] Y. Zhou, J. Tan, D. Chong, X. Wan, J. Zhang, *Adv. Funct. Mater.* **2019**, *29*, 1901202.
[21] J. Liao, J. Huang, S. Yang, X. Wang, T. Wang, W. Sun, Z. Tong, *ACS Appl. Polym. Mater.* **2019**, *1*, 2703.
[22] L. Du, Z.-Y. Xu, C.-L. Huang, F.-Y. Zhao, C.-J. Fan, J. Dai, K.-K. Yang, Y.-Z. Wang, *Appl. Mater. Today* **2020**, *18*, 100463.
[23] D. Chi, H. Gu, J. Wang, C. Wu, R. Wang, Z. Cheng, D. Zhang, Z. Xie, Y. Liu, *Mater. Horiz.* **2023**, *10*, 2464.
[24] L. S. Novelino, Q. Ze, S. Wu, G. H. Paulino, R. Zhao, *Proc. Natl. Acad. Sci., U.S.A.* **2020**, *117*, 24096.
[25] X. Yan, Q. Zhou, M. Vincent, Y. Deng, J. Yu, J. Xu, T. Xu, T. Tang, L. Bian, Y.-X. J. Wang, K. Kostarelos, L. Zhang, *Sci. Robot.* **2017**, *2*, eaaq1155.
[26] Z. Zhang, J. T. Heron, A. Pena-Francesch, *Adv. Funct. Mater.* **2023**, *33*, 2215248.
[27] Y. Lee, F. Koehler, T. Dillon, G. Loke, Y. Kim, J. Marion, M.-J. Antonini, I. C. Garwood, A. Sahasrabudhe, K. Nagao, X. Zhao, Y. Fink, E. T. Roche, P. Anikeeva, *Adv. Mater.* **2023**, *35*, 2301916.
[28] S. Qi, H. Guo, J. Fu, Y. Xie, M. Zhu, M. Yu, *Compos. Sci. Technol.* **2020**, *188*, 107973.
[29] B. Sun, R. Jia, H. Yang, X. Chen, K. Tan, Q. Deng, J. Tang, *Adv. Intell. Syst.* **2022**, *4*, 2100139.
[30] J. Yan, J. J. Mecholsky, K. B. Clifton, *Bone* **2007**, *40*, 479.
[31] E. F. Morgan, H. H. Bayraktar, T. M. Keaveny, *J. Biomech.* **2003**, *36*, 897.
[32] D. Taylor, N. O'Mara, E. Ryan, M. Takaza, C. Simms, *J. Mech. Behav. Biomed. Mater* **2012**, *6*, 139.
[33] B. C. W. Kot, Z. J. Zhang, A. W. C. Lee, V. Y. F. Leung, S. N. Fu, *PLoS One* **2012**, *7*, e44348.
[34] J. Van Kuilenburg, M. A. Masen, E. Van Der Heide, *Proc. Inst. Mech. Eng., Part J.* **2013**, *227*, 349.
[35] A. Steed, E. Ofek, M. Sinclair, M. Gonzalez-Franco, *Nat. Commun.* **2021**, *12*, 4758.
[36] M. S. Kim, Y. Lee, J. Ahn, S. Kim, K. Kang, H. Lim, B.-S. Bae, I. Park, *Adv. Funct. Mater.* **2023**, *33*, 2208792.
[37] D. Han, Y. Zhang, X. Y. Zhang, Y. M. Xie, X. Ren, *Compos. Struct.* **2023**, *311*, 116849.
[38] K. K. Dudek, J. A. I. Martínez, G. Ulliac, M. Kadic, *Adv. Mater.* **2022**, *34*, 2110115.
[39] Z. Yan, F. Zhang, J. Wang, F. Liu, X. Guo, K. Nan, Q. Lin, M. Gao, D. Xiao, Y. Shi, *Adv. Funct. Mater.* **2016**, *26*, 2629.
[40] H. Zhao, X. Cheng, C. Wu, T.-L. Liu, Q. Zhao, S. Li, X. Ni, S. Yao, M. Han, Y. Huang, Y. Zhang, J. A. Rogers, *Adv. Mater.* **2022**, *34*, 2109416.
[41] S. Xu, Z. Yan, K.-I. Jang, W. Huang, H. Fu, J. Kim, Z. Wei, M. Flavin, J. McCracken, R. Wang, A. Badea, Y. Liu, D. Xiao, G. Zhou, J. Lee, H. U. Chung, H. Cheng, W. Ren, A. Banks, X. Li, U. Paik, R. G. Nuzzo, Y. Huang, Y. Zhang, J. A. Rogers, *Science* **2015**, *347*, 154.
[42] D. Rus, M. T. Tolley, *Nat. Rev. Mater.* **2018**, *3*, 101.
[43] D. Melancon, B. Gorissen, C. J. García-Mora, C. Hoberman, K. Bertoldi, *Nature* **2021**, *592*, 545.
[44] F. Feng, X. Dang, R. D. James, P. Plucinsky, *J. Mech. Phys. Solids* **2020**, *142*, 104018.
[45] X. Xin, L. Liu, Y. Liu, J. Leng, *Adv. Funct. Mater.* **2020**, *30*, 2004226.
[46] Y. Chi, Y. Li, Y. Zhao, Y. Hong, Y. Tang, J. Yin, *Adv. Mater.* **2022**, *34*, 2110384.
[47] S. Rahman, L. Wu, A. El Elmi, D. Pasini, *Adv. Funct. Mater.* **2023**, *33*, 2304151.